Crystal structure of the Ca^{2+}-form and Ca^{2+}-binding kinetics of metastasis-associated protein, S100A4.

Alexandre R. Gingras[1], Jaswir Basran[1], Andrew Prescott[1], Marina Kriajevska[2], Clive R. Bagshaw[1], and Igor L. Barsukov[3*]

[1] Department of Biochemistry, University of Leicester, Henry Wellcome Building, Leicester LE1 9HN, UK

[2] Department of Cancer Studies and Molecular Medicine, University of Leicester, Hodgkin Building, Leicester LE1 9HN, UK

[3] School of Biological Sciences, University of Liverpool, BioSciences Building, Liverpool L69 7ZB, UK

* Correspondence author. Email address: I.Barsukov@liverpool.ac.uk

Abstract

S100A4 takes part in control of tumour cell migration and contributes to metastatic spread in *in vivo* models. In the active dimeric Ca^{2+}-bound state it interacts with multiple intracellular targets. Conversely, oligomeric forms of S100A4 are linked with the extracellular function of this protein. We report the 1.5 Å X-ray crystal structure of Ca^{2+}-bound S100A4 and use it to identify the residues involved in target recognition and to derive a model of the oligomeric state. We applied stopped-flow analysis of tyrosine fluorescence to derive kinetics of S100A4 activation by Ca^{2+} (k_{on} = 3.5 $\mu M^{-1}.s^{-1}$, k_{off} = 20 s^{-1}).

Keywords: S100A4, Ca^{2+}-binding, ligand binding, crystal structure, kinetics, tyrosine fluorescence

1. Introduction

The Ca^{2+}-binding protein S100A4 belongs to the S100 protein family, which includes at least 25 members that have a similar EF-hand structure and participate in various cellular processes as transducers of Ca^{2+} signals [1,2]. S100A4 is a protein associated with metastatic progression in different tumour types [3,4]. Recently, up-regulation of S100A4 was described in various carcinoma cell lines undergoing an epithelial-mesenchymal transition [5]. In a number of cell models, experimental modulation of S100A4 expression levels directly affects the migratory abilities of cells [2]. The intracellular functions of S100A4 are associated with the dimeric structure, whereas the oligomeric form has an extracellular role [6,7]. In spite of structural similarities between different S100 family members, their intracellular and extracellular targets are different [1,8]. This is particularly pronounced for S100A4, S100A6 and S100B that have higher sequence homology to each other than to other members of the S100 family. The large number of ligands [9] makes it particularly important to identify general structural features of the S100 proteins that affect selectivity as structure determination for all possible complexes is impractical, or even impossible. The detailed analysis has been reported recently for S100B targets focusing on the properties of the ligands [10], but no systematic comparison has been done for the binding sites of the proteins.

The majority of S100 ligands bind to the active Ca^{2+} form of the proteins. S100A4 binds two Ca^{2+} ions per mol monomer with μM affinity [11,12]. Dukhanina et al. [11] reported a mean value of the K_d = 2.6 μM with no evidence of cooperativity between sites within a monomer nor within the dimer. From NMR chemical shift data, Dutta et al. [12] considered that the pseudo EF-hand (N-terminal site 1) bound Ca^{2+} with slightly higher affinity than the canonical EF-hand (C-terminal site 2). Other authors have considered that the high affinity site only involves site 2 and binding to site 1 is very weak (K_d > 500 μM) [13], but this would not match the reported stoichiometry of other studies [11,12].

The high-resolution structure of the apo S1004 has been determined by NMR [14] and the structure of the Ca^{2+}-bound form has been suggested based on that of S100B [15]. However the sequence variations at the ligand binding site make the model unreliable for the analysis of S100A4 interactions with targets. Here we report on the crystal structure of Ca^{2+}-bound S100A4 at 1.5 Å resolution and use this structure, in conjunction with the published structures of S100A6 and S100B, to identify the key residues involved in target recognition. In addition, the interaction between the S100A4 dimers in the asymmetric unit provides a model for the formation of tetramers and higher order oligomers that are important for biological activity of S100A4. We used stopped-flow measurements to establish the kinetics of Ca^{2+} binding that leads to the conversion of S100A4

into the active state.

2. Materials and methods

2.1 X-Ray crystallography

S100A4 was cloned into the pQE30 vector (Qiagen, U.K.) that adds non-cleavable N-terminal 6 His-tag and expressed in BL21 (DE3) strain of E.coli. The protein was purified using standard affinity and gel-filtration protocols. Crystals of human Ca^{2+}-bound S100A4, residues 1-101, were obtained at 20°C by vapour diffusion using 40% (w/v) PEG 600, 100 mM CHES (pH 9.5). Protein at 40.0 mg/ml in 20 mM MES pH 7.0, 50 mM NaCl, 10 mM $CaCl_2$ was mixed with an equal volume of precipitant. Crystals belong to space group P32 with cell dimensions of *a,b*=52.3 Å, *c*=139.1 Å, α,β=90º, and γ=120º. The crystal contained 4 molecules per asymmetric unit, or 2 dimers, with a solvent content of 41.3%.

Native data sets were collected at ESRF, beamline ID14-3 (λ=0.931), using an ADSC Quantum 4 detector. Data sets were indexed and reduced with XDS [16]. The structure was solved by molecular replacement using Phaser with the bovine Ca^{2+}-bound S100B structure used as a search model (PDB ID 1mho). The first map was of reasonable quality and the model was improved using manual building with Coot and maximum likelihood refinement using Refmac5 [17].
The model converged to an R_{work} of 19.5% and R_{free} of 21.8% for all data between 50 and 1.5Å. The final Ramachandran plot showed 90.5% of residues in favoured regions, 9.5% in additional favoured regions as defined by PROCHECK [18]. The structure has been submitted to the Protein Data Bank with the accession number 3c1v (www.rcsb.org). During manuscript preparation a similar crystal structure (r.m.s.d. 0.4 Å) of the Ca^{2+}-form of S100A4 was released (PDB ID 2q91). Figures were generated with CCP4mg and PyMol (www.pymol.org).

2.2 Fluorescence spectroscopy

Protein (tyrosine) fluorescence was recorded using an SLM 8000 spectrofluorimeter (Urbana, U.S.A). Stopped-flow fluorescence measurements were carried out using an Applied Photophysics SM18MV instrument (Leatherhead, U.K.). Tyrosine fluorescence was measured by excitation at 280 nm and the emission was selected with WG305 and UG11 filters (Comar, U.K.). Reactions were measured in 20 mM NaCl, 10 mM HEPES, 2 mM DTT , (± 1mM $MgCl_2$) at pH 7.5 and 20°C. The S100A4 monomer concentration was calculated using an A_{280} of 3,000 M^{-1} cm^{-1}.based on the tyrosine content.

3. Results and discussion

3.1 Structure of Ca-bound S100A4

Crystals (250 x 120 x 70 μm) that diffracted X-rays to 1.5 Å resolution were obtained for S100A4 in the presence of $CaCl_2$. The crystal structure was determined from a single crystal using molecular replacement. The asymmetric unit contains two S100A4 dimers with all four monomers having virtually identical conformations (average r.m.s.d. for backbone atoms 0.4 Å). The main difference between the monomers is the orientations of long side-chains of solvent exposed residues. The overall fold of the monomer follows establish topology of S100 proteins and consists of two Ca^{2+}-binding helix-loop-helix motifs, N-terminal pseudo EF-hand and C-terminal canonical EF-hand. The two Ca^{2+}-binding motifs are separated by a well-ordered loop containing a helical turn (Fig. 1A, B). The dimer is stabilised by extensive hydrophobic interactions between side-chains from helices 1 and 4 of each monomer burying 22% (1481 $Å^2$) of the total surface area of each monomer.

Ca^{2+} in site 1 is coordinated by the backbone carbonyl groups of S20, E23, D25, and K28, the side chain carbonyl of E33 and a water molecule (Fig. 1D). This binding site is formed at the C-terminal end on the helix 1 and requires minimal structural rearrangement on complex formation as follows from the comparison with the structure of the apo form [14]. Ca^{2+} coordination in site 2 involves carbonyl groups of E69 backbone and N65 side chain, side chain carboxyl groups of D63, D67, and E74 and a water molecule. This binding site is formed by the H3-H4 loop and requires a large structure rearrangement on complex formation. The two Ca^{2+}-binding sites are close in space and a hydrophobic contact forms between the aliphatic parts of the K28 from site 1 and E69 from site 2.

The structure of the Ca^{2+}-form of S100A4 is very close to the reported structures of S100A6 (PDB index 1K9K) and S100B (PDB index 1MHO) as illustrated in Fig. 1C. The conformations of the Ca^{2+}-binding motifs and their relative orientation are identical in the three proteins, as follows from the high sequence homology (Fig. 1A). The majority of the residues involved in Ca^{2+}-binding and interactions between the helices are identical or conserved. The main sequence and structural differences between the three proteins are associated with the loop between the Ca^{2+}-binding motifs (Fig. 1A-C). In S100A4 this loop contains a helical turn that is brought into the close contact with the helices H3 and H4 through the hydrophobic interaction involving side chains of F45 and L46. As the result, the loop forms a bottom part of a triangle (in the orientation of Fig. 1C) with the other two sides formed by H3 and H4. The hydrophobic side chains from the loop fill the gap between the two helices, thus creating an extensive flat hydrophobic surface. In S100B a similar helical turn is also formed but has a different orientation that creates a deeper hydrophobic pocket than that of S100A4. The S100A6 sequence has a two-residue deletion in the loop region removing F45 altogether and creating a short highly twisted structure. Overall, despite the sequence variations in

the H2-H3 loop region, all structures feature the extension of the hydrophobic surface between the helices H3 and H4 through the addition on the hydrophobic residues from the loop. However, the configuration of the resulting surface is significantly different between the three proteins, providing the basis for the target specificity.

3.2 Ligand binding and oligomerisation interface

The conformations of S100 proteins undergo very limited structural changes on target binding compared with the Ca^{2+}-bound structure. This allows us to rationalise the target specificity from the comparison of S100A4 structure with the structures of S100A6 and S100B that have high sequence homology, similar overall structures but interact with distinct sets of ligands [9]. The combined binding surface for different S100 ligands maps to a continuous area of S100A4 structure that includes H2-H3 loop and adjacent sides of the helices H3 and H4, as illustrated in Fig. 2A. This conclusion is based on the S100B/p53 (PDB 1DT7), S100B/NDR kinase (PDB 1PSB) and S100A10, S100A11/annexin (PDB 1BT6 and 1QLS) complexes (see Fig. 1A for residues involved in binding). Strikingly, the non-conserved residues of the S100 sequences in Fig. 1A are concentrated predominantly in or in the close proximity to the combined binding surface as illustrated in Fig. 2 B and C. Although some of the variability away from the binding surface is likely caused by the lack of an evolutionary pressure, the variations at the binding site reflect target specificity.

The binding areas in each S100A4, S100A6 and S100B monomer consist of an extensive hydrophobic patch surrounded by a small number of charged groups as shown in Fig. 2D-F. The shape of the surface and the charge distributions are distinctly different for these proteins, in agreement with different target specificity. Sequence comparison of Fig. 1A identifies residues that have the largest effect on the properties of the binding surface. Substitutions that lead to the change of the surface profile while maintaining its hydrophobic property, involve F45 (deletion in S100A6), C81(A,M) (residues in brackets correspond to S100A6 and S100B, respectively), M86(I,A) C87(Y,C) and F89(A, F). Substitutions of this type affect complementarity between the protein and the ligand, resulting in the atomic clashes between S100A4 and modelled ligands from other S100 proteins, as can be seen in Fig. 2A. Another small group of substitutions lead to the change in the charge distribution. These include D10(G,V), G47(G,E), R49(K,I), A51(A,E), A52(E,V) and N61(D,T). As non-complimentary of surfaces or charges would prevent complex formation, the residues listed above create the basis for target selectivity of S100A4. The limited number of the residues makes these good candidates for mutations aimed at the selectivity modification.

The two dimers of the asymmetric unit are positioned close to each other and for the two

adjacent monomers we observed additional electron density corresponding to the C-terminal region 92-98. This region makes a specific extended contact with the ligand binding surface of the monomer from another dimer, resulting in a symmetric tetramer as illustrated in Fig. 2H. The interaction shows surface and charge complementarity illustrated in Fig. 2I with the R49-E91 ion pair formation and hydrophobic contacts L48-F93, F45-P94 and F78-P98. The peptide lies flat across the ligand binding surface over the area similar to that of p53, as illustrated in Figs 1A and 2I, covering 13% (889 $Å^2$) of accessible surface area of each monomer. The C-termini of the non-contacting monomers are exposed and available for further interactions, making possible the formation of higher oligomers. This model of self-association agrees with simultaneous detection of tetramers and higher oligomeric structures important for interaction with some of the S100A4 targets [7,8]. The absence of the C-terminal tetramerisation region in S100B leads to a different oligomerisation model that involves direct extensive contacts between helices H1, H4 and H2-H3 loop, favouring the formation of an octamer [19].

The S100A4 C-terminal sequence complimentary to the target recognition surface is ^{91}ExFPxxxP^{98} (Fig. 2H). This sequence has a high resemblance to the C-terminal region of the myosin IIA sequence ^{1926}DLPFVVP^{1932} reported to be important for the interaction with S100A4 [20]. The differences in the two sequences are likely to improve the complementarity as the replacement of Pro (S100A4) with Phe (myosin) would favour the stacking interaction with F45 (S100A4), while Pro residue in the myosin sequence can still maintain the hydrophobic interaction with L48 (S100A4). In addition, the hydrophobic side chains of Val residues can make contacts with the neighbouring hydrophobic surfaces of the loop L2 and the helix H3. Further structural and binding studies are needed for the full understanding of S100A4 interaction with targets.

3.3 Ca^{2+} binding kinetics

S100A4 lacks tryptophan and therefore the protein fluorescence is dominated by tyrosine emission (λ_{em} = 310 nm) from Y19 and Y75. Saturating Ca^{2+} concentrations (>100 μM) caused an 8% quench in tyrosine emission. The dissociation rate constant was determined to be 20 s^{-1} by mixing S100A4 in the presence of saturating Ca^{2+} with an excess of EGTA (Fig. 3A). This reaction was unaffected by the addition of 1 mM Mg^{2+}, indicating that the tyrosine is monitoring Ca^{2+} dissociation from specific site(s) rather than Ca^{2+}/Mg^{2+} sites [21]. The association rate constant is more complicated to determine because the S100A4 is likely to have some bound Ca^{2+} in equilibrium with contaminant Ca^{2+} in the buffer. Addition of excess EGTA (effective K_d = 0.026 μM at pH 7.5) renders the S100A4 essentially Ca^{2+} free. When mixed with a larger excess of Ca^{2+} in the stopped -flow instrument, the Ca^{2+} binding process could be monitored via the quench in tyrosine fluorescence (Fig. 3B). At an added Ca^{2+} of >180 μM, the observed rate constant became

linearly dependent on added Ca^{2+} to reveal an association rate constant of 3.6 $\mu M^{-1}.s^{-1}$ (Fig. 3C). Combining this value with the dissociation rate constant yields a K_d of 5.5 μM. From the amplitude of the fluorescence change as a function of added Ca^{2+}, the stoichiometry and K_d were obtained as 1.77 ± 0.18 Ca^{2+}/monomer and 4.4 ± 2.2 μM respectively (Fig. 3D). This result indicates both site 1 and site 2 are occupied by Ca^{2+}. The signal-to-noise of the tyrosine fluorescence records is insufficient to resolve small (i.e. within 4 fold) differences in binding to site 1 and 2 and thus the estimated K_d^{obs} could represent a geometric mean = $\sqrt{K_d^{I} . K_d^{II}}$) of the individual sites. Analysis of Fig. 4 of Dutta et al. [12] indicates that the ratio of K_d values of site 2 compared with site 1 is between 3 and 7, based on the change in chemical shift of V70 (site 2) relative to L29 and G24 respectively (site 1) at intermediate occupancy with Ca^{2+}.

The aromatic ring of Y19 is positioned between the helices H1 and H2 and with one side of the ring fully exposed to solvent in the apo form. In Ca^{2+}-bound state the helix H2 moves closer to the aromatic ring, partially shielding it from solvent and making a contact with the buried face of the ring. The change in the orientation of the helix is caused by the large move of the adjacent helix H3 caused by Ca^{2+} binding in site 2. The aromatic ring of Y75 is buried in both forms and undergoes minimal change in environment. Thus we suggest that the observed changes in fluorescence are associated with Y19 in response to Ca^{2+} binding in site 2. This prediction is being tested by site-directed mutagenesis. Target binding is expected to favour Ca^{2+} binding [11] and preliminary studies indicate that a myosin IIA C-terminal fragment reduces the Ca^{2+} dissociation rate constant for the S100A4-Ca^{2+} complex by more than 30 fold. The kinetics of Ca^{2+} binding and release indicate that S100A4 would respond to intracellular Ca^{2+} spikes that typically last a few seconds.

Acknowledgements

We thank Juhwan Kim and Arathi Mohan for assistance in protein preparation and fluorescence measurements. This work was funded by the BBSRC.

References

[1] Donato, R. (2007) RAGE: a single receptor for several ligands and different cellular responses: the case of certain S100 proteins. Curr Mol Med 7, 711-24.

[2] Tarabykina, S., Griffiths, T.R.L., Tulchinsky, E., Mellon, J.K., Bronstein, I.B. and Kriajevska, M. (2007) Metastasis-associated protein S100A4: spotlight on its role in cell migration. Curr. Cancer Drug Targets 7, 217-228.

[3] Helfman, D.M., Kim, E.J., Lukanidin, E. and Grigorian, M. (2005) The metastasis associated protein S100A4: role in tumour progression and metastasis. Br J Cancer 92,

1955-8.

[4] Garrett, S.C., Varney, K.M., Weber, D.J. and Bresnick, A.R. (2006) S100A4, a mediator of metastasis. J Biol Chem 281, 677-80.

[5] Mejlvang, J., Kriajevska, M., Berditchevski, F., Bronstein, I., Lukanidin, E.M., Pringle, J.H., Mellon, J.K. and Tulchinsky, E.M. (2007) Characterization of E-cadherin-dependent and -independent events in a new model of c-Fos-mediated epithelial-mesenchymal transition. Exp Cell Res 313, 380-93.

[6] Dulyaninova, N.G., Malashkevich, V.N., Almo, S.C. and Bresnick, A.R. (2005) Regulation of myosin-IIA assembly and Mts1 binding by heavy chain phosphorylation. Biochemistry 44, 6867-76.

[7] Novitskaya, V., Grigorian, M., Kriajevska, M., Tarabykina, S., Bronstein, I., Berezin, V., Bock, E. and Lukanidin, E. (2000) Oligomeric forms of the metastasis-related Mts1 (S100A4) protein stimulate neuronal differentiation in cultures of rat hippocampal neurons. J Biol Chem 275, 41278-86.

[8] Kiryushko, D., Novitskaya, V., Soroka, V., Klingelhofer, J., Lukanidin, E., Berezin, V. and Bock, E. (2006) Molecular mechanisms of Ca(2+) signaling in neurons induced by the S100A4 protein. Mol Cell Biol 26, 3625-38.

[9] Santamaria-Kisiel, L., Rintala-Dempsey, A.C. and Shaw, G.S. (2006) Calcium-dependent and -independent interactions of the S100 protein family. Biochem J 396, 201-14.

[10] Wilder, P.T., Lin, J., Bair, C.L., Charpentier, T.H., Yang, D., Liriano, M., Varney, K.M., Lee, A., Oppenheim, A.B., Adhya, S., Carrier, F. and Weber, D.J. (2006) Recognition of the tumor suppressor protein p53 and other protein targets by the calcium-binding protein S100B. Biochim Biophys Acta 1763, 1284-97.

[11] Dukhanina, E.A., Dukhanin, A.S., Lomonosov, M.Y., Lukanidin, E.M. and Georgiev, G.P. (1997) Spectral studies on the calcium-binding properties of Mts1 protein and its interaction with target protein. FEBS Lett 410, 403-6.

[12] Dutta, K., Cox, C.J., Huang, H., Basavappa, R. and Pascal, S.M. (2002) Calcium coordination studies of the metastatic Mts1 protein. Biochemistry 41, 4239-45.

[13] Garrett, S.C., Hodgson, L., Rybin, A., Toutchkine, A., Hahn, K.M., Lawrence, D.S. and Bresnick, A.R. (2008) A biosensor of S100A4 metastasis factor activation: inhibitor screening and cellular activation dynamics. Biochemistry 47, 986-96.

[14] Vallely, K.M., Rustandi, R.R., Ellis, K.C., Varlamova, O., Bresnick, A.R. and Weber, D.J. (2002) Solution structure of human Mts1 (S100A4) as determined by NMR spectroscopy. Biochemistry 41, 12670-80.

[15] Tarabykina, S., Scott, D.J., Herzyk, P., Hill, T.J., Tame, J.R., Kriajevska, M., Lafitte, D.,

Derrick, P.J., Dodson, G.G., Maitland, N.J., Lukanidin, E.M. and Bronstein, I.B. (2001) The dimerization interface of the metastasis-associated protein S100A4 (Mts1): in vivo and in vitro studies. J Biol Chem 276, 24212-22.

[16] Kabsch, W. (1993) Automatic processing of rotation diffraction data from crystals of initially unknown symmetry and cell constants. J. Appl. Cryst. 26, 795-800.

[17] Murshudov, G.N., Vagin, A.A. and Dodson, E.J. (1997) Refinement of macromolecular structures by the maximum-likelihood method Acta Cryst. D53, 240-255.

[18] Laskowski, R.A., Macarthur, M.W., Moss, D.S. and Thornton, J.M. (1993) PROCHECK - a program to check the stereochemical quality of protein structures. J. Appl. Cryst. 26, 283-291.

[19] Ostendorp, T., Leclerc, E., Galichet, A., Koch, M., Demling, N., Weigle, B., Heizmann, C.W., Kroneck, P.M. and Fritz, G. (2007) Structural and functional insights into RAGE activation by multimeric S100B. EMBO J 26, 3868-78.

[20] Kriajevska, M., Tarabykina, S., Bronstein, I., Maitland, N., Lomonosov, M., Hansen, K., Georgiev, G. and Lukanidin, E. (1998) Metastasis-associated Mts1 (S100A4) protein modulates protein kinase C phosphorylation of the heavy chain of nonmuscle myosin. J Biol Chem 273, 9852-6.

[21] Bagshaw, C.R. and Reed, G.H. (1977) The significance of the slow dissociation of divalent metal ions from myosin 'regulatory' light chains. FEBS Lett 81, 386-90.

Figure Legends

Fig. 1. Structure of Ca^{2+}-bound S100A4 and comparison with other proteins. (A) Sequence alignments of S100A4, S100A6 and S100B. The location of the secondary structure elements in S100A4 structure are shown above the sequence. Ca^{2+}-coordinated residues are highlighted in green, residues involved in tetramerisation - in red, p53 binding – in blue, annexin binding – in yellow. (B) Ribbon representation of the S100A4 structure. S100-hand is marked in orange, EF-hand in pale yellow, H2-H3 loop in green. Ca^{2+} ions are represented as red balls. (C) Superposition of monomer structures of S100A4 (orange), S100A6 (magenta) and S100B (cyan). (D,E) Stereo view of Ca^{2+} binding sites with electron density, Ca^{2+} represented by green balls. Site 1 (D) and Site 2 (E).

Fig. 2. S100A4 ligand recognition and tetramerisation sites. (A) Areas involved in ligand binding from reported S100 complexes mapped on the surface of S100A4. p53 binding to S100B is shown in blue (1DT7) with additional region from S100B/NDR kinase complex (1PSB) shown in cyan. Annexin binding to S100A10 (1BT6) and S100A11 (1QLS) is shown in yellow. Orientations of the peptides are shown as Cα-traces, p53 in red, NDR in orange, annexin in magenta. To generate the mapping and position the peptides the corresponding complexes were superimposed on the structure of S100A4. (B,C) Non-conserved residues between S100A4, S100A6 and S100B sequences mapped on the surface of S100A4. B and C views differ by the 180^{o} rotation around their vertical axes. (D-F) Comparison of electrostatic potentials at the binding sites of S100A4 (D), S100A6 (E) and S100B (F). (G) Tetramerisation contacts observed for S100A4 in the crystal form. The expansion of the boxed area is shown in (H) for details. (I) Position of the C-terminal tetramerisation domain at the S100A4 ligand binding site. The orientation of the ribbon diagram corresponds to the orientations of all the surface representations for comparison, excluding (C).

Fig. 3. Ca^{2+} binding to S100A4 monitored by tyrosine fluorescence. (A) Dissociation of Ca^{2+} (k_{obs} = 20 s^{-1}) observed by mixing 13 μM S100A4 + 100 μM $CaCl_2$ against 200 μM EGTA. (B) Association of Ca^{2+} (k_{obs} = 140 s^{-1}) observed on mixing 20 μM S100A4 + 100 μM EGTA against 180 μM $CaCl_2$. (C) The observed rate constant as a function of added Ca^{2+} concentration. At ≤100 μM added Ca^{2+} no signal was observed as the Ca^{2+} was sequestered by EGTA. Above 160 μM Ca^{2+} the observed rate constant become linear with added $[Ca^{2+}]$, yielding a second order association rate constant of 3.6 $\mu M^{-1}.s^{-1}$. (D) The amplitude of the observed transients in (C) plotted as a function of added $[Ca^{2+}]$. The data were fitted to a quadratic equation to reveal a B_{max} = 36 μM Ca^{2+} and a K_d =

4.4 μM. Reaction chamber concentrations are stated throughout.

TABLE I Crystallographic analysis and refinement statistics on the Ca^{2+}-bound S100A4.

Data collection	
Space group	P32
Cell dimensions	*a*,*b* = 52.32 Å, *c* = 139.14 Å α,β = 90°, γ = 120°
No. of molecules in a.u.	4 (2 dimers)
Wavelength (Å)	0.931
Resolution (Å)	50-1.5
Measured reflections	260418
Unique reflections	68427
Completeness (%)	99.5 (98.9)
R_{sym}	10.2 (44.8)
I/σI	9.46 (3.14)
Refinement statistics	
Resolution range (Å)	50-1.5 (1.539-1.5)
Unique reflections (free)	64569 (3409)
R_{work} (%)	19.5 (23.9)
R_{free} (%)	21.8 (26.4)
Number of residues	380
Number of Calcium	8
Number of solvent molecules	552
Average B value ($Å^2$)	16.5
Rmsd bond length (Å)	0.006
Rmsd bond angles (Å)	0.965
ESU based on R value (Å)	0.106
ESU based on R_{free} value (Å)	0.081

R_{sym} = Σ|I-<I>|ΣI, I is the observed intensity and <I> is the average intensity of the multiple observations of symmetry-related reflections. R = Σ||Fo|-|Fc||Σ|Fo|; R_{free} is calculated for a randomly-selected 5% of the reflections; R_{factor} is calculated for the remaining 95% of the reflections used in refinement. Values in brackets represent the outer resolution shell. ESU = Estimated Standard Uncertainties.

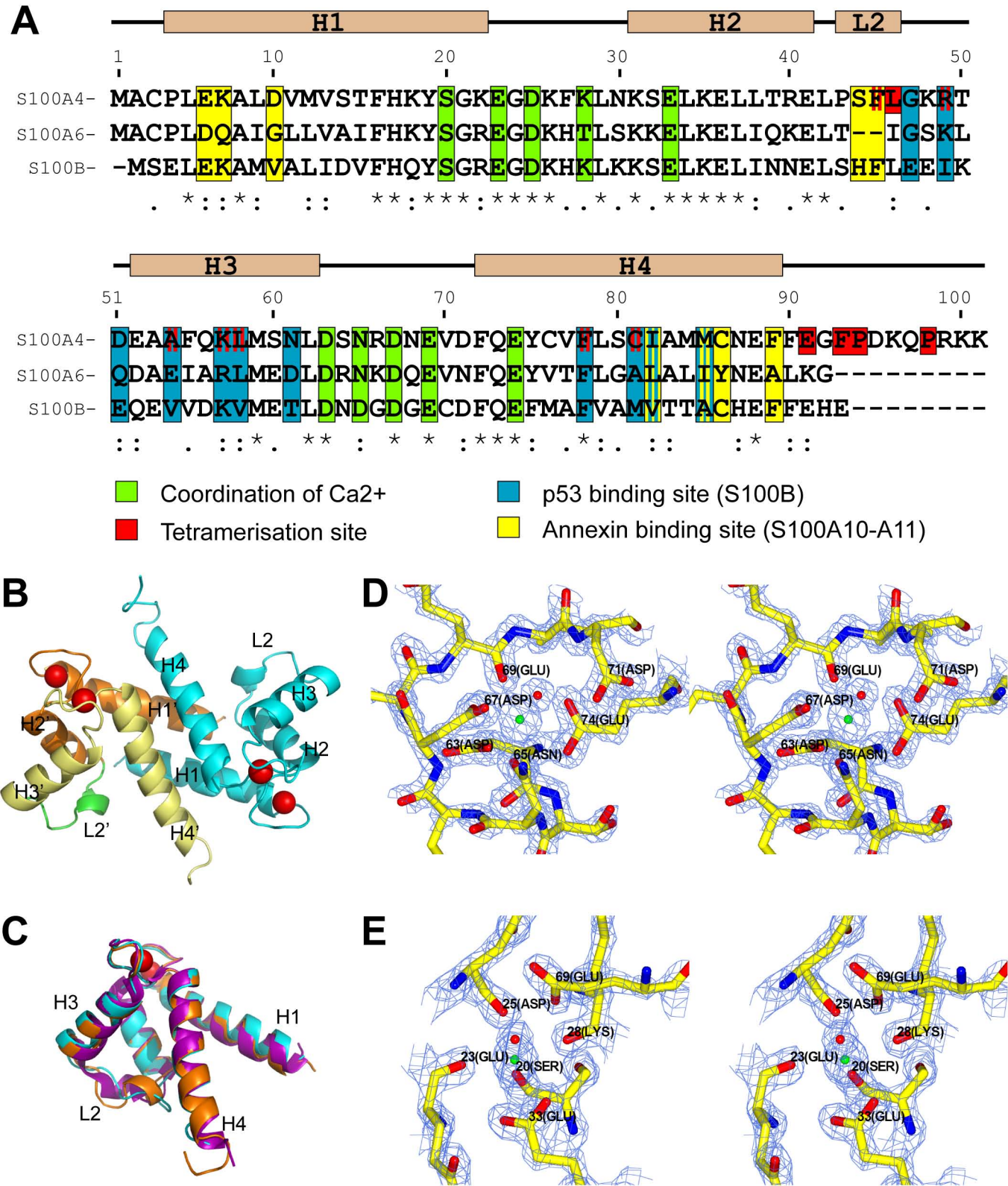
A
H1
H2
L2
H3
H4
S100A4-
S100A6-
S100B-
Coordination of Ca2+
Tetramerisation site
p53 binding site (S100B)
Annexin binding site (S100A10-A11)
B
L2
H4
H3
H1'
H2'
H2
H1
H3'
L2'
H4'
C
H3
H1
L2
H4
D
69(GLU)
71(ASP)
67(ASP)
74(GLU)
63(ASP)
65(ASN)
E
69(GLU)
25(ASP)
28(LYS)
23(GLU)
20(SER)
33(GLU)

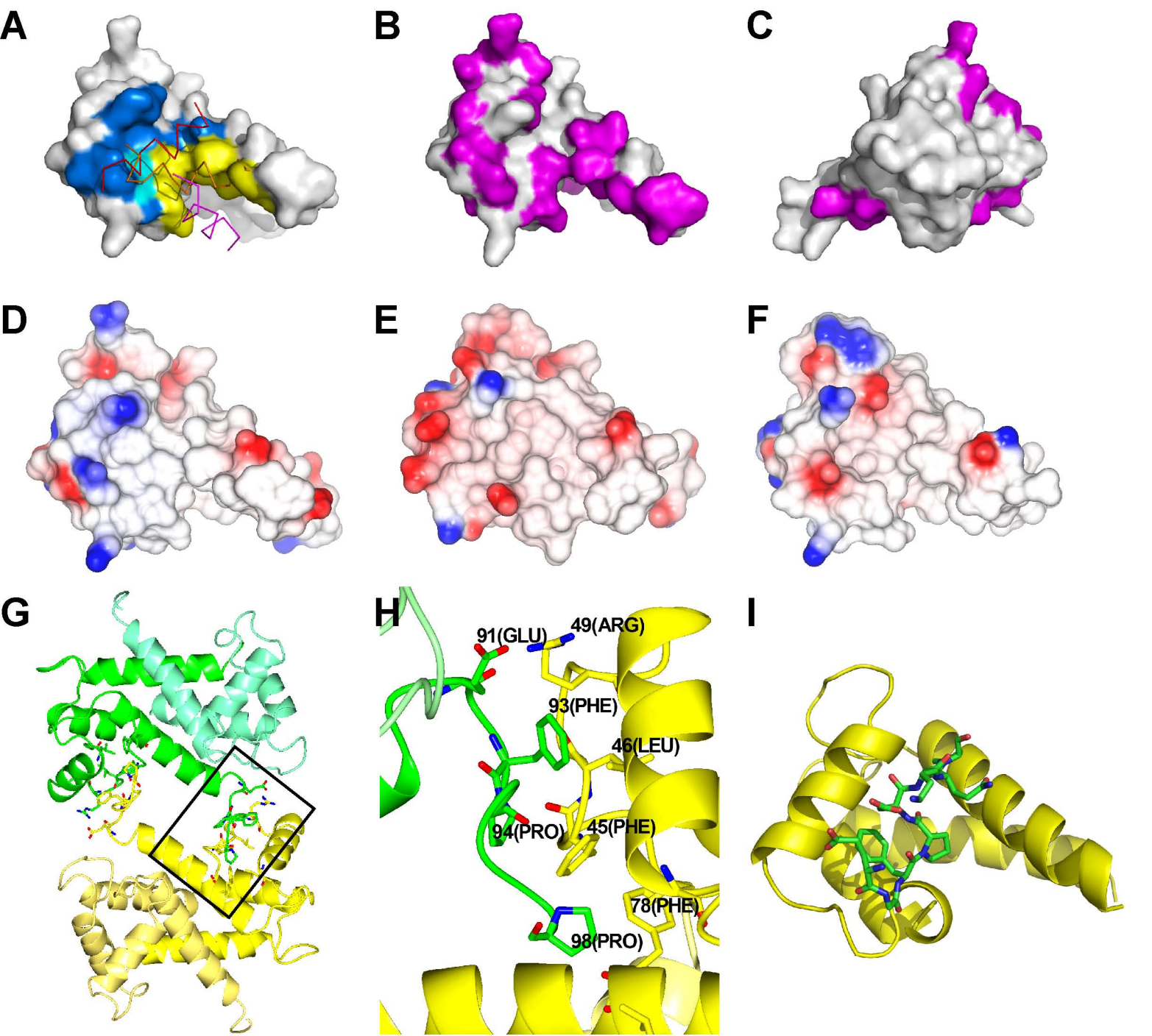
A
B
C
D
E
F
G
H
I
91(GLU)
49(ARG)
93(PHE)
46(LEU)
94(PRO)
45(PHE)
78(PHE)
98(PRO)

Figure 3

(A)

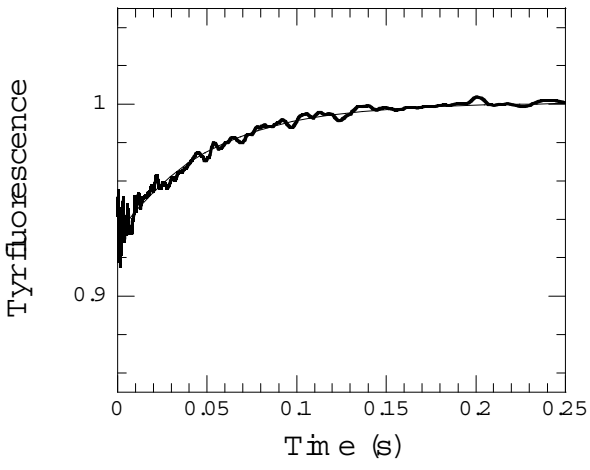

(B)

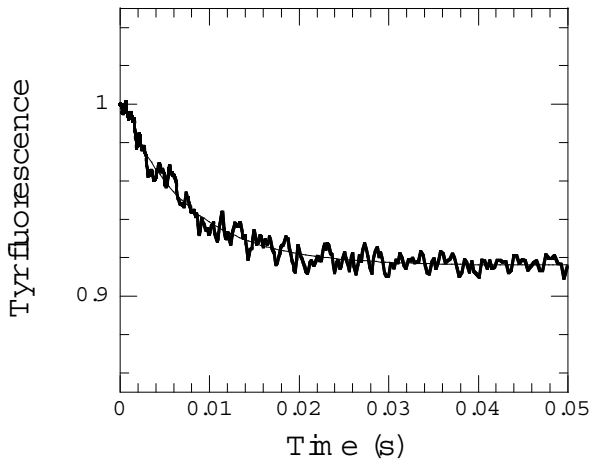

(C)

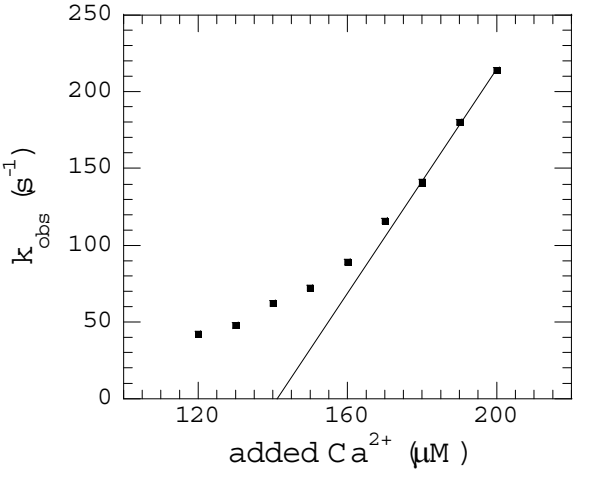

(D)